All-optical hysteresis control by means of cross-phase modulation in semiconductor optical amplifiers

Drew N. Maywar and Govind P. Agrawal

The Institute of Optics, University of Rochester, Rochester, New York

Yoshiaki Nakano

Department of Electronic Engineering, University of Tokyo, Tokyo, Japan

Received August 31, 2000; revised manuscript received February 12, 2001

We describe the principle of operation of an all-optical flip-flop based on dispersive bistability in a distributed feedback semiconductor optical amplifier. Cross-phase modulation controls the photonic bandgap and Bragg resonances of the amplifier, thereby shifting the hysteresis and switching thresholds to higher or lower powers. We give the details of a simple theoretical model that is used to simulate the set and reset operations. We also experimentally investigate the dependence on set-signal power and the response to back-to-back set signals, and we apply the theoretical model to understand these experimental results. © 2001 Optical Society of America

OCIS codes: 250.5980, 070.4340, 050.1950, 060.4510, 190.1450, 200.4560.

1. INTRODUCTION

Optical signals that experience a nonlinear refractive index while interacting with a diffraction grating can exhibit dispersive bistability.[1,2] Feedback from the grating (commonly called distributed feedback, or DFB) creates Bragg resonances, at wavelengths that depend on the nonlinear refractive index. Bistable switching occurs when changes in signal power shift a Bragg resonance through the signal wavelength, thereby reinforcing the power change and creating a positive feedback loop.[3]

In semiconductor optical amplifiers (SOAs), the refractive index depends significantly on the carrier density.[4] Optical signals that deplete the carrier density experience a strong nonlinear refractive index with an effective $n_2 \sim 10^{-9}\ \mathrm{cm}^2/\mathrm{W}$ (Ref. 5), which is seven orders of magnitude greater than the Kerr nonlinearity of silica fibers. In addition to this strong nonlinearity, SOAs exhibit inherent gain, are compact, and are capable of integration, making them appealing as building blocks of functional photonic gates.[6,7]

Exploiting the SOA carrier-induced nonlinearity for dispersive bistability, researchers have realized an all-optical flip-flop,[8,9] in which a built-in Bragg grating can be used for feedback (in place of Fabry–Perot facet reflections) to allow integration onto a single substrate with other photonic gates.[2,10] The two output states of the flip-flop are simply where the signal's input power P_H intersects the two branches of the hysteresis curve, as shown in Fig. 1. The output power of the signal can be set and reset between P_{on} and P_{off} by varying P_H through the upward and downward switching thresholds, respectively.[8]

Recently, set and reset techniques were demonstrated in which auxiliary optical signals were used; and in which the holding-beam input power P_H remained constant.[10] The separation of holding and control functionality is advantageous because it allows the holding-beam source to be optimized solely for wavelength and power stability. Furthermore, set and reset can then be performed directly by signals from an optical network. The new control techniques are based on cross-phase modulation (XPM) and therefore possess a wide wavelength range of operation (set range of >35 nm and reset range of >160 nm[10]); hence, control signals can come from a variety of wavelength channels in modern-day wavelength-division multiplexed systems, in which the channel spacing is ~0.8 nm.

This paper describes the XPM-based control techniques by using a theoretical model, and it applies this model to an experimental investigation into set-pulse effects. In Section 2, we develop a model of the bistable system (composed of the holding beam, index grating, and SOA carrier nonlinearity), and we simulate the set and reset operations by varying the holding-beam input power P_H. Auxiliary control signals are introduced into the model in Section 3, where we show how flip-flop operation is achieved by varying the bistable hysteresis curve. In Section 4, the model is used to explain our experimental investigation into the flip-flop's dependence on the set-signal power and its response to back-to-back set signals.

2. BISTABLE SYSTEM

The time-dependent theoretical study of dispersive bistability in DFB SOAs must account for the carrier-density dynamics and the bistable signals's interaction with the carrier density and the diffraction grating. A model incorporating these features was previously presented,[2] and

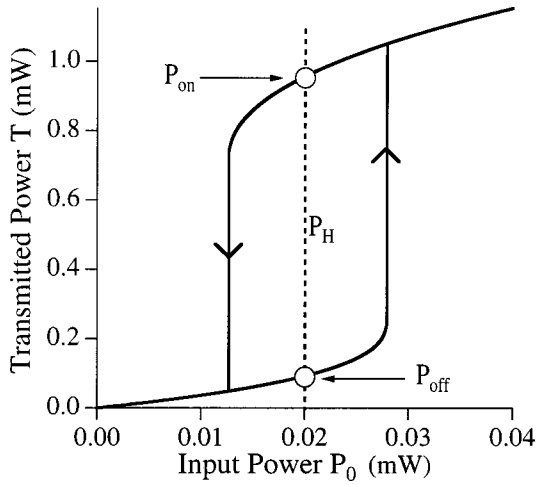

Fig. 1. Bistable hysteresis curve. Two stable transmission states, P_{on} and P_{off}, occur for a single input power P_H.

it was used to study pulses that undergo bistable switching. In this section, we describe equations that govern the bistable system, along with a solution and its approximations; this presentation facilitates the description of the all-optical flip-flop, and it is the starting point for incorporating auxiliary control signals into the model. This incorporation is addressed in Section 3.

The optical field $\mathbf{E}$ that undergoes bistability within the DFB SOA can be expressed as

$$\mathbf{E}(x,y,z,t) = \mathrm{Re}\{\hat{\epsilon}F(x,y)[A(z,t)\exp(i\beta_B z) + B(z,t)\exp(-i\beta_B z)]\exp(-i\omega t)\}, \quad (1)$$

where Re{ } represents the real part, $\hat{\epsilon}$ is the unit vector along the transverse-electric orientation of polarization, $F(x,y)$ is the transverse-mode distribution, and ω is the optical frequency. In the longitudinal direction (z coordinate), the field scatters off of the index grating and is therefore conveniently expressed as two counterpropagating terms; A and B are the slowly varying field envelopes for the forward- and backward-propagating fields, respectively, and the Bragg wave number $\beta_B = \pi/\Lambda$ is related inversely to the grating period Λ.

The propagation of the electric field is described, in general, by a wave equation. Representing the grating as a periodic dielectric function,[11] the wave equation leads to the following coupled-mode equations for the field envelopes:

$$\frac{\partial A}{\partial z} + \frac{1}{v}\frac{\partial A}{\partial t} = i\left[\delta - i\frac{g}{2}(1 - i\alpha) + i\frac{\alpha_{\mathrm{int}}}{2}\right]A + i\kappa B, \quad (2)$$

$$-\frac{\partial B}{\partial z} + \frac{1}{v}\frac{\partial B}{\partial t} = i\left[\delta - i\frac{g}{2}(1 - i\alpha) + i\frac{\alpha_{\mathrm{int}}}{2}\right]B + i\kappa A. \quad (3)$$

Here v is the group velocity, g is the gain experienced by the optical modes, α_{int} accounts for internal losses, and κ is the coupling coefficient representing the index grating. The contribution of spontaneous emission is not included because the amplified optical signal is expected to be much stronger. The mismatch between the optical signal wave number and the Bragg wave number β_B is partly accounted for by the detuning parameter $\delta = \beta_0 - \beta_B$, where β_0 is the carrier-density-independent portion of the signal's wave number β_N.

The carrier-density-*dependent* portion of the real part of the optical wave number is given by $\beta_N = -\alpha g/2$. The linewidth-enhancement factor α couples changes in gain to the refractive index, both of which are functions of the carrier density N (Ref. 4); α represents the nonlinearity that gives rise to dispersive bistability in this system. Considering a linear change in gain ($a = \mathrm{d}g/\mathrm{d}N$) and refractive index ($b = \mathrm{d}n/\mathrm{d}N$) with respect to the carrier density N, we can express the linewidth-enhancement factor as $\alpha = -2(\omega/c)(b/a)$, where c is the speed of light in vacuum. The gain g experienced by the optical modes is related to the carrier density N by[4]

$$g(x,y,z,t) = a\Gamma[N(x,y,z,t) - N_0], \quad (4)$$

where N_0 is the carrier density at transparency, Γ is the optical confinement factor and represents the fraction of the transverse intensity distribution $|F(x,y)|^2$ that falls within the gain-region area Wd, and W and d are the width and thickness of the gain region, respectively.

The carrier density N is the density of electron-hole pairs, and we assume charge neutrality between the conduction-band electrons and valence-band holes.[4] The carrier density amplifies the optical signal via stimulated emission and affects its wave number and optical phase, and therefore it plays a key role in optical bistability. For time scales much longer than the intraband relaxation time ($\sim$0.05 ps), the dynamics of the carrier density in both SOAs and semiconductor lasers has been successfully modeled by a rate equation[4]

$$-D\nabla^2 N + \frac{\partial N}{\partial t} = \frac{J}{ed} - \frac{N}{\tau} - a(N - N_0)\frac{I}{\hbar\omega}, \quad (5)$$

where D is the diffusion coefficient, and the right-hand side consists of various mechanisms that create or recombine electron-hole pairs. The first terms represents electrical injection of carriers, where J is the injected current density and e is the electric charge. The second term accounts for spontaneous and nonradiative recombination mechanisms, where τ is the carrier lifetime; we neglect the carrier-density dependence of τ to simplify our analysis.[7] The final term accounts for stimulated recombination of electron-hole pairs by the optical signal, where $\hbar\omega$ is the photon energy, $I = \langle \mathbf{E}\cdot\mathbf{E}\rangle_t$ is the optical intensity, and $\langle\rangle_t$ indicates temporal averaging over many optical periods $2\pi/\omega$.

The carrier rate equation can be simplified considerably by noting that the diffusion length ($\approx 2\ \mu$m) is longer than the gain-region thickness $d \sim 0.15\ \mu$m and width $W \sim 2\ \mu$m (for an index-guided device). Thus, the average value of the carrier density is used in the transverse dimensions; averaging rate equation (5) over the active-region area Wd yields

$$\frac{\mathrm{d}N}{\mathrm{d}t} = \frac{J}{ed} - \frac{N}{\tau} - \frac{a}{\hbar\omega}(N - N_0)\frac{\Gamma\sigma}{Wd}(|A|^2 + |B|^2), \quad (6)$$

where N is now understood to be averaged over the transverse dimensions, $\Gamma = \int_0^W\int_0^d \mathrm{d}x\,\mathrm{d}y|F(x,y)|^2/\sigma$ is the optical confinement factor, and $\sigma = \int_{-\infty}^{\infty}\int_{-\infty}^{\infty}\mathrm{d}x\,\mathrm{d}y|F(x,y)|^2$ is

the mode cross section. Carrier diffusion, which has been dropped from Eq. (6), is also assumed to smooth out the spatial holes burned by counterpropagating fields (typical period $\approx 0.2\ \mu$m), allowing the intensity interference terms to be neglected. The carrier density is assumed to otherwise vary slowly enough that the product $D\partial^2 N/\partial z^2$ is negligible.

Because the carrier density enters the coupled-mode equations through the modal gain g, it is convenient to formulate a gain rate equation by using Eqs. (6) and (4):

$$\tau \frac{\mathrm{d}g}{\mathrm{d}t} = g_0 - \left[1 + \frac{P_A + P_B}{P_{\mathrm{sat}}}\right] g. \tag{7}$$

The quantity $g_0 = \Gamma a N_0(\bar{J} - 1)$ is the small-signal value of g, $\bar{J} = J\tau/edN_0$ is the current density normalized to its value required to achieve transparency, $P_A = |A|^2\sigma$ and $P_B = |B|^2\sigma$ are the optical powers of the individual envelopes, and $P_{\mathrm{sat}} = \hbar\omega W d/(\tau a \Gamma)$ is the saturation power.

Gain rate equation (7) can be simplified by assuming that the average value of the optical power is sufficient to calculate the saturated gain.[2,12] Using the mean power, and assuming a uniform electrical bias J, we find that the gain itself no longer varies along the amplifier. An equation for the uniform gain can be derived by averaging rate equation (7) over the length of the amplifier L:

$$\tau \frac{\mathrm{d}\langle g\rangle}{\mathrm{d}t} = g_0 - \left[1 + \frac{\langle P_A\rangle + \langle P_B\rangle}{P_{\mathrm{sat}}}\right]\langle g\rangle, \tag{8}$$

where the angled brackets indicate longitudinal averaging. For the final term, we have factored the average of the gain–power products into the average of their arguments; such a factoring scheme is referred to as the mean-field approximation.[13]

The powers P_A and P_B in Eq. (8) are obtained from the coupled-mode equations; analytic solutions are possible if we apply some common assumptions. Under the approximation that the average power is sufficient to calculate the gain (as discussed above), the gain becomes uniform along the amplifier, and we may use its average value $\langle g\rangle$ in the coupled-mode equations.[2,12] This is a sensible approximation for uniform-grating DFB SOAs because the combined intensity of the counterpropagating coupled modes can result in a nearly uniform saturated-gain distribution.[2]

To further simplify the coupled-mode equations, we assume that the field envelopes A and B adjust instantaneously to changes in the SOA gain.[2,14] The optical fields therefore attain their steady state quickly (allowing the time derivatives to be dropped), and the system dynamics are determined solely by Eq. (8). This adiabatic approximation is valid when the unobstructed signal-transit time through the amplifier ($L/v_g \approx 0.003$ ns) is much shorter than the carrier lifetime ($\tau \approx 0.2$–1 ns), and when it is shorter than the rise and fall of the input-field envelope $h(t)$.

Under the adiabatic and uniform-gain approximations, coupled-mode equations (2) and (3) become ordinary differential equations (of independent variable z) with constant coefficients. The general solutions for the counterpropagating fields are then[4]

$$A = A_1 \exp(i\gamma z) + rB_2 \exp(-i\gamma z), \tag{9}$$

$$B = q^{-1}A_1 \exp(i\gamma z) + B_2 \exp(-i\gamma z), \tag{10}$$

where $\gamma = \sqrt{\Delta^2 - \kappa^2}$, $\Delta = \delta - (i/2)\langle g\rangle(1 - i\alpha) + i(\alpha_{\mathrm{int}}/2)$, $r = (\gamma - \Delta)/\kappa$, and $q = (-\gamma - \Delta)/\kappa$. Applying the boundary conditions of an input-field envelope $h(t)$ at one facet, that is, $A(z = -L/2, t) = h(t)$ and $B(z = L/2, t) = 0$, and assuming that antireflection coatings nullify the facet reflections, we find that the solutions are

$$A = h\,\frac{\gamma\cos(\gamma\xi) + i\Delta\sin(\gamma\xi)}{\gamma\cos(\gamma L) - i\Delta\sin(\gamma L)}, \tag{11}$$

$$B = h\,\frac{i\kappa\sin(\gamma\xi)}{\gamma\cos(\gamma L) - i\Delta\sin(\gamma L)}, \tag{12}$$

where $\xi = z - L/2$.

Using field envelopes (11) and (12), we find that optical powers P_A and P_B are

$$P_A = P_0\zeta[\cosh(2\gamma_i\xi)\theta_1 - \sinh(2\gamma_i\xi)\theta_2 + \cos(2\gamma_r\xi)\theta_3 - \sin(2\gamma_r\xi)\theta_4], \tag{13}$$

$$P_B = P_0\zeta|\kappa|^2[\cosh(2\gamma_i\xi) - \cos(2\gamma_r\xi)], \tag{14}$$

where $P_0(t) = |h(t)|^2\sigma$ is the input power, $\gamma = \gamma_r + i\gamma_i$, $\theta_1 = \gamma\gamma^* + \Delta\Delta^*$, $\theta_2 = \gamma\Delta^* + \gamma^*\Delta$, $\theta_3 = \gamma\gamma^* - \Delta\Delta^*$, $\theta_4 = i(\gamma\Delta^* - \gamma^*\Delta)$, and $\zeta = [\cosh(2\gamma_i L)\theta_1 + \sinh(2\gamma_i L)\theta_2 + \cos(2\gamma_r L)\theta_3 + \sin(2\gamma_r L)\theta_4]^{-1}$.

To obtain the average power within the SOA, we integrate solutions (13) and (14) over the device length L to yield

$$\langle P_A\rangle = P_0\zeta\left\{\frac{\sinh(2\gamma_i L)\theta_1 + [\cosh(2\gamma_i L) - 1]\theta_2}{2\gamma_i L} + \frac{\sin(2\gamma_r L)\theta_3 + [1 - \cos(2\gamma_r L)]\theta_4}{2\gamma_r L}\right\}, \tag{15}$$

$$\langle P_B\rangle = P_0\zeta|\kappa|^2\left[\frac{\sinh(2\gamma_i L)}{2\gamma_i L} - \frac{\sin(2\gamma_r L)}{2\gamma_r L}\right]. \tag{16}$$

Substituting average powers (15) and (16) into gain rate equation (8) adiabatically eliminates the internal optical powers; the resulting ordinary differential equation has only a single dependent variable, $\langle g\rangle$, and is relatively simple to solve numerically (we have used a variable-order technique for the simulations shown here). Once the average gain $\langle g\rangle$ is calculated for all time, the solution can be used to obtain the bistable output power.

Analytic expressions for the bistable transmitted power $T(t) = P_A(z = L/2, t)$ and reflected power $R(t) = P_B(z = -L/2, t)$ can be found by using Eqs. (13) and (14), respectively:

$$T = P_0\zeta 2(\gamma_r^2 + \gamma_i^2), \tag{17}$$

$$R = P_0\zeta|\kappa|^2[\cosh(2\gamma_i L) - \cos(2\gamma_r L)]. \tag{18}$$

The transmitted-power expression (17) was used to generate Fig. 1, where $\kappa L = 3$, $\alpha = 5$, $g_0 L = 1.19815$ ($\approx$95% lasing threshold), and $P_{\mathrm{sat}} = 10$ mW, common values used throughout this paper. The internal loss α_{int} commonly ranges from 10 to 50 cm^{-1}, depending on the amplifier design. However, the particular choice of α_{int}

does not affect the physical process of hysteresis control; we choose $\alpha_{\text{int}}L = 0$ to simplify the following discussion. To trace out the hysteresis curve, we used a sinusoidal input power $P_0(t) = p\{1 - \cos[2\pi t/T_m]\}$, where $p = 0.6\,\text{mW}$ is the input amplitude, and $T_m = 10^6\tau$ is the modulation period. When the input–output transfer function (P_0 versus T) is plotted, explicit time dependence does not exist; arrowheads have been added to Fig. 1 to indicate the direction of power change in time. Because the purpose of the figure is to show the two stable states corresponding to a single input power P_H, we selected a long modulation period T_m that produces a familiar-looking shape of the hysteresis curve. The correspondingly large integration step size $\Delta t = 100\tau$ skips over transient behavior at the switching thresholds. Such behavior is not central to our discussions regarding the stable output states [Figs. 1, 3, 4, and 7(b)], but it is included in the context of flip-flop operation (Figs. 2, 5, and 9 below).

For the bistable system to be used as a flip-flop, the input power P_0 is initially located between the switching thresholds, like P_H in Fig. 1. Optical set can be performed by increasing the input power beyond the upward switching threshold[8,9] and can be understood as follows. An increase in optical power within the SOA stimulates recombination of electron-hole pairs (i.e., gain saturation), which increases the refractive index; the signal thereby increases its own wave number and optical phase. This self-phase modulation (SPM) shifts the photonic bandgap and Bragg resonances to longer wavelengths. As a Bragg resonance moves onto the signal wavelength, the internal optical power increases even more. Bistable upward switching occurs when a positive feedback loop (among the internal optical power, nonlinear refractive index, and Bragg resonance) causes the Bragg resonance to shift through the signal wavelength, providing resonant amplification for the signal.[3] Set operation is shown in Fig. 2, where the input power is given by $P_0 = P_H[1 + 0.5f(t - t_1) - 0.5f(t - t_2)]$, $P_H = 0.02\,\text{mW}$ is the mean input power, $f(t - t_x) = \exp\{-[(t - t_x)/W_f]^{2Q}\}$, $t_1 = 23\,\text{ns}$, $t_2 = 63\,\text{ns}$, $W_f = 1\,\text{ns}$, $\tau = 0.2\,\text{ns}$ (a common value used throughout), $Q = 4$ is the order of the super-Gaussian-shaped perturbation in the holding power, and $\Delta t = 2\,\text{ps}$.

The signal's output power remains at a high level P_{on} (corresponding to the upper hysteresis branch) even after its input power returns to the initial state P_H, as shown in Fig. 2. Although the bistable signal provides the same input power, the larger output is achieved because the new Bragg-resonance location provides resonant amplification. The larger optical power within the SOA, in turn, maintains the amount of carrier-density depletion required to lock the Bragg resonance in place.

The flip-flop is reset by decreasing the input power of the holding beam beyond the downward switching threshold of the hysteresis curve. The resulting decrease in the internal optical power allows the carrier density to recover, thereby *decreasing* the refractive index. SPM shifts the Bragg resonance to shorter wavelengths and back toward the holding-beam wavelength. As the resonance peak passes the signal wavelength, a positive feedback loop (acting in the opposite manner as for upward switching) shifts the Bragg resonance to even shorter wavelengths and lowers the output power to P_{off}.[3] In terms of the input power P_0, reset is achieved by the application of a "negative" optical pulse,[8] as shown in Fig. 2.

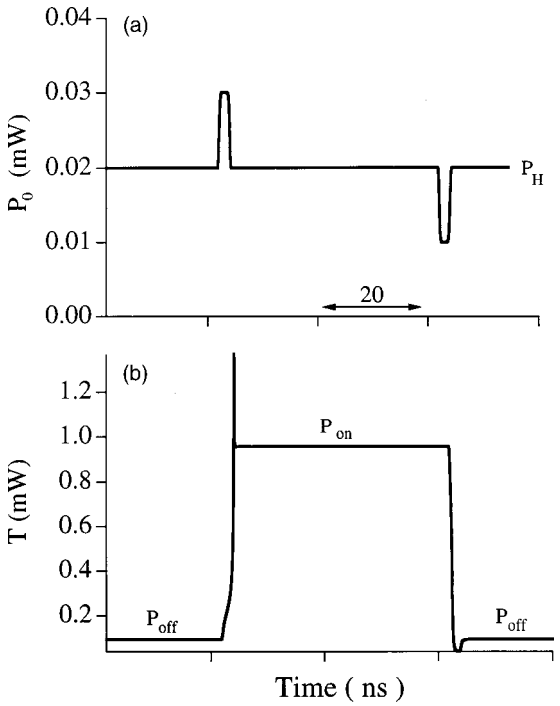

Fig. 2. Flip-flop operation based on the holding beam: (a) The holding-beam input power P_0 is varied beyond the switching thresholds to (b) set and reset its bistable transmission T.

3. CONTROL SIGNALS

For the flip-flop operation described in Section 2, the holding beam provides the power used to latch the flip-flop *and* initiates set and reset by means of SPM. These control functions, however, can be delegated to auxiliary signals; holding-beam SPM is then replaced by control-signal XPM.

The set signal, like the holding beam, falls within the SOA gain spectrum and hence stimulates recombination of electron-hole pairs. Recombination causes gain saturation and increases the refractive index *even* at the holding-beam wavelength. Thus, the set signal modulates the wave number and phase of the holding beam; this kind of XPM has been used in other geometries and applications, including data-wavelength conversion in SOA-integrated Mach–Zehnder interferometers,[15] and clock recovery and clock division in nonlinear optical-loop mirrors.[7]

For our application, the increase in refractive index pushes the photonic bandgap and Bragg resonances to longer wavelengths. Upward switching occurs when the Bragg resonance has been shifted sufficiently to seed the positive feedback loop discussed in Section 2. In terms of the hysteresis curve, using XPM to shift the Bragg resonance toward the holding-beam wavelength corresponds to pushing the switching thresholds to lower powers.

Switching, as depicted in Fig. 3, occurs once the upward-switching threshold has been brought to the holding-beam input power P_H.

After the set pulse passes through the SOA, the hysteresis curve returns to its initial shape, but now the output power falls on the higher branch at P_{on}, as depicted in Fig. 3. The postswitching location of the Bragg resonance provides resonant amplification of the holding beam, resulting in larger output power and sufficient internal power to lock the resonance in place, as described in Section 2.

The flip-flop is reset by pushing the hysteresis curve to higher powers, allowing the downward-switching threshold to reach the holding-beam input power, as depicted in Fig. 4. The hysteresis curve can be shifted in this way by signals that are *absorbed* by the SOA, giving their energy to electrons that are then excited into the semiconductor conduction band. This gain pumping is accompanied by a *decrease* in the refractive index and optical phase at the holding-beam wavelength. Thus, the sign of XPM for the reset signals is opposite that of the set signals. As the refractive index decreases, the Bragg resonance shifts to shorter wavelengths; reset occurs when the Bragg resonance shifts enough to cause the positive feedback loop described in Section 2.

XPM-based reset is qualitatively different from SPM-based reset; the former increases the carrier density directly by the application of optical power (i.e., a "positive" optical pulse). For SPM-based reset, in contrast, the carrier density increases through the natural recovery of the SOA gain as the internal power is reduced. The internal holding-beam power can be reduced either by using a negative optical pulse (as shown in Fig. 2)[8] or by interfering the holding beam with a closely tuned auxiliary signal.[9] The interfering-signal technique shifts the bistable switching thresholds to higher powers while the holding-beam input power remains constant and can be achieved at relatively low reset-beam powers, but it requires the holding and reset wavelengths to match closely (~0.008 nm). In contrast, the XPM-based reset technique can be achieved over a wide wavelength range (>160 nm), but it requires higher powers (>0.7 mW).[10]

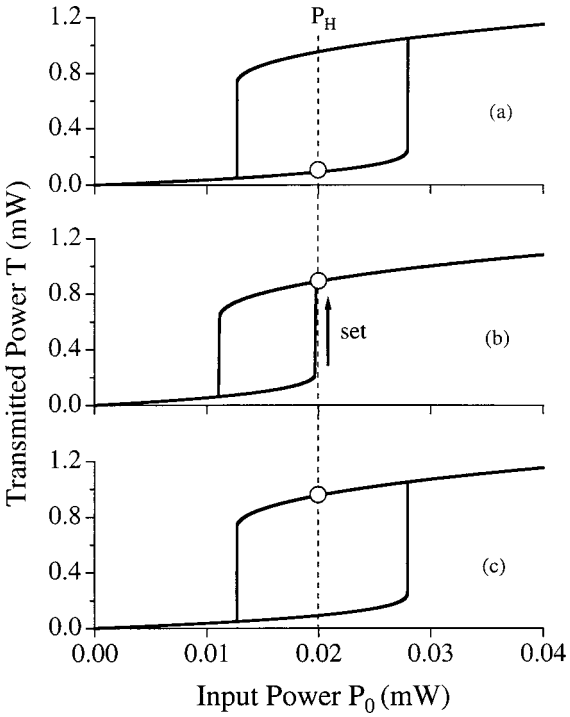

Fig. 3. XPM-based set: (a) the transmitted power (indicated by the circle) is initially low for a fixed input power P_H. (b) XPM ($+\Delta\phi$) caused by a set signal pushes the hysteresis curve to smaller powers, thereby switching the transmission to a higher power. (c) After the set signal passes, the hysteresis curve relaxes to its initial shape, with the transmitted-power state on the higher hysteresis branch.

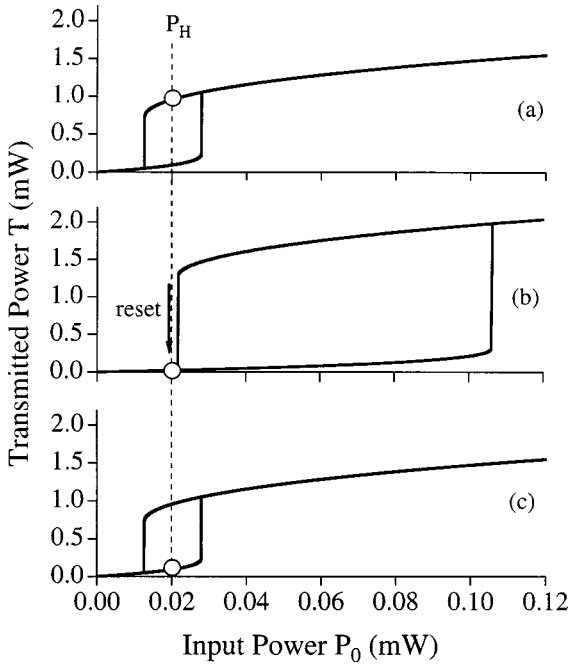

Fig. 4. XPM-based reset: (a) high initial transmitted power (indicated by the circle). (b) XPM ($-\Delta\phi$) caused by a reset signal pushes the hysteresis curve to larger powers, and the transmitted power drops to a lower hysteresis curve branch. (c) Hysteresis curve relaxes to its initial shape, and transmission remains at the lower power.

Our goal in modeling the XPM set–reset techniques is to show hysteresis control and flip-flop operation by incorporating the control signals in a simple, phenomenological manner. The set $\mathbf{E}_S$ and reset $\mathbf{E}_R$ fields pass through the DFB SOA without interacting with the index grating, and they can be expressed as

$$\mathbf{E}_S(x,y,z,t) = \mathrm{Re}\{\hat{\epsilon}F(x,y)S(z,t)\exp(i\beta_S z)\exp(-i\omega_S t)\}, \quad (19)$$

$$\mathbf{E}_R(x,y,z,t) = \mathrm{Re}\{\hat{\epsilon}F(x,y)R(z,t)\exp(i\beta_R z)\exp(-i\omega_R t)\}. \quad (20)$$

The polarization vector $\hat{\epsilon}$ and transverse field $F(x,y)$ are assumed to be the same as those of the holding beam, S and R are the slowly varying field envelopes, and β_S and β_R are the wave numbers. The set-signal optical frequency ω_S falls within the SOA gain curve, and the reset-signal frequency ω_R falls outside the gain curve, on the higher-frequency side.

The control signals affect the bistable output power of the holding beam by changing the SOA carrier density; we include these signals into the model by expanding rate equation (5) as

$$-D\nabla^2 N + \frac{\partial N}{\partial t} = \frac{J}{ed} - \frac{N}{\tau} - a(N - N_0)\frac{I}{\hbar\omega} - a(N - N_0)\frac{I_S}{\hbar\omega_S} + \eta\frac{I_R}{\hbar\omega_R}. \quad (21)$$

The first three terms on the right-hand side are found in rate equation (5) of Section 2. The penultimate term accounts for stimulated recombination of electron-hole pairs by the set signal having an intensity I_S. The final term accounts for the reset signal, having an intensity I_R, and η characterizes its absorption by the valence-band electrons.

The set-signal term within rate equation (21) is similar to the holding-beam term, in that both deplete the carrier density. In general, the amount of gain experienced by these signals will depend on their detuning from the SOA gain peak, the spectral location of which shifts with changes in the carrier density. We ignore these gain-curve-dependent effects for this simple model.

Interference terms involving the set signal were also dropped. Nonlinear frequency mixing is negligible from the submilliwatt input powers used in experiments. In addition, we have avoided the close detuning (0.008 nm) between the set and holding beam in our experiments that can reset the flip-flop (as discussed in Section 2). Spatial interference was neglected because carrier diffusion is assumed to smooth out the longitudinal spatial holes.

To account for carrier generation by the reset signal, we consider the SOA to be an ideal four-level system. The reset-signal photons are absorbed by electrons occupying the first level (bottom of the valence band). These electrons jump to the fourth level (top of the conduction band), where they quickly relax (<1 ps) to the third level (bottom of conduction band) and become part of the carrier density N. Thus, the absorbed photon flux $\eta I/(\hbar\omega_R)$ in Eq. (21) represents a transfer of energy from the reset signal to the carrier density. To simplify our study, we assume that this energy-transfer process has perfect efficiency, and we ignore the depletion of the ground-state electrons (i.e., η is constant). The increase in gain that is due to the reset-signal term in the gain rate equation resembles J/ed, which accounts for the electrical injection of carriers.

We simplify Eq. (21) in the same manner as discussed in Section 2 for Eq. (5). Averaging over the transverse dimensions of the active region introduces the optical confinement factor Γ and the mode cross section σ; because the transverse model distribution $F(x, y)$ is assumed to be the same for holding beam and the control fields, the confinement factor Γ and mode cross section σ are also identical. We also assume that the average optical power is sufficient to calculate the carrier density, and we invoke the mean-field approximation. Using gain expression (4), we find that the resulting gain rate equation is

$$\tau\frac{d\langle g\rangle}{dt} = g_0 + \eta\frac{\langle P_R\rangle}{P_{R\mathrm{sat}}} - \left[1 + \frac{\langle P_A\rangle + \langle P_B\rangle}{P_{\mathrm{sat}}} + \frac{\langle P_S\rangle}{P_{S\mathrm{sat}}}\right]\times\langle g\rangle, \quad (22)$$

where $P_S = |S|^2\sigma$, $P_R = |R|^2\sigma$, $P_{S\mathrm{sat}} = \hbar\omega_S Wd/(\tau a\Gamma)$, and $P_{R\mathrm{sat}} = \hbar\omega_R Wd/(\tau a\Gamma)$.

The control signal powers P_S and P_R can be obtained from the following propagation equations,

$$\frac{\partial P_S}{\partial z} + \frac{1}{v_S}\frac{\partial P_S}{\partial t} = gP_S, \quad (23)$$

$$\frac{\partial P_R}{\partial z} + \frac{1}{v_R}\frac{\partial P_R}{\partial t} = -\eta P_R, \quad (24)$$

where v_S and v_R are the group velocities for the set and reset signals, respectively. As in Section 2, we assume that the SOA responds to the average signal power, which allows the modal gain g to be replaced by its average value $\langle g\rangle$. This is a more severe approximation for the control signals than for the holding beam because the former do not scatter off of the grating and therefore have an exponential variation in z. Nonetheless, eliminating the z dependence of such traveling-wave signals is a common simplification used in the study of nonlinear phenomena in SOA's,[7] and it is especially suited for a qualitative analysis and for a relatively small gain–length product.

Propagation equations (23) and (24) can be simplified further by assuming that the control signals respond instantaneously to changes in the carrier density. As for the holding signal, this adiabatic approximation is valid when the transit time through the amplifier ($L/v_x \approx 0.003$ ns) is much shorter than both the carrier lifetime ($\tau \approx 0.2$–1 ns) and the rise and fall of the input-field envelopes. The control-signal equations become

$$\frac{dP_S}{dz} = \langle g\rangle P_S, \quad (25)$$

$$\frac{dP_R}{dz} = -\eta P_R. \quad (26)$$

Applying the boundary conditions $P_S(z = -L/2, t) = P_{S0}(t)$ and $P_R(z = -L/2, t) = P_{R0}(t)$, we find that the solutions to Eqs. (25) and (26) give the control-signal distributions along the amplifier:

$$P_S = P_{S0}\exp\left[g\left(z + \frac{L}{2}\right)\right], \quad (27)$$

$$P_R = P_{R0}\exp\left[-\eta\left(z + \frac{L}{2}\right)\right]. \quad (28)$$

Integrating Eqs. (27) and (28) over the length of the amplifier, we obtain

$$\langle P_S\rangle = P_{S0}\frac{\exp(gL) - 1}{gL}, \quad (29)$$

$$\langle P_R\rangle = P_{R0}\frac{1 - \exp(-\eta L)}{\eta L}. \quad (30)$$

A short control pulse (e.g., ~8 ps) can abruptly change the carrier density on a scale much smaller than τ (e.g., a few picoseconds[7]), thus invalidating the adiabatic elimination of the optical signals over this time interval. After such an abrupt change, however, the carrier density recovers at a rate governed by the carrier lifetime τ, the time scale used for the adiabatic approximation, and our model regains its validity. The validity of the adiabatic approximation can also be threatened by a *slowly* varying set signal and even by the continuous-wave (CW) holding beam itself. By operating these signals at high powers, the carrier density responds to an effective carrier lifetime $\tau_{\text{eff}} = \tau/(1 + P_I/P_{\text{sat}})$,[7] which can approach the signal transit time (≈3 ps). The internal power P_I in our simulations, however, does not exceed the saturation power, so our model remains valid for the cases considered here.

Our model is now complete. The control-signal powers (27) and (28) are used within modified gain rate equation (22). Once the gain is calculated for all time, the solution vector is used to find the holding-beam output powers using Eqs. (17) and (18), derived in Section 2.

We used this model to show how the hysteresis curve shifts in Fig. 3 and 4 under the application of CW set and reset signals, respectively. The initial and final hystereses [parts (a) and (c)] are identical to the hysteresis curve of Fig. 1, and they do not include control signals. The same parameter values are used in Fig. 3(b), except for a CW set signal with $P_{S0} = 84\,\mu\text{W}$ and $P_{S\text{sat}} = 10\,\text{mW}$. For Fig. 4(b), this set signal was replaced by a reset signal defined by $P_{R0} = 1.2\,\text{mW}$, $P_{R\text{sat}} = 11.8\,\text{mW}$, with $\eta L = 2.3$.

The model correctly simulates the behavior of the all-optical flip-flop; namely, the set signal switches the holding beam to a higher output-power state, which is maintained longer than the set-pulse width, and the holding-beam power returns to its lower state upon the application of the reset pulse. As an example, we use input control pulses of the form

$$P_{S0}(t) = S_i \exp\{-[(t - t_S)/W_S]^{2M}\}, \tag{31}$$

$$P_{R0}(t) = R_i \exp\{-[(t - t_R)/W_R]^{2N}\}, \tag{32}$$

where S_i and R_i are the input amplitudes, t_S and t_R define the center of the pulses, W_S and W_R are proportional to the pulse widths, and M and N are the orders of the super-Gaussian pulses. Flip-flop operation is shown in Fig. 5, where the control signals are defined by $S_i = 0.1\,\text{mW}$, $R_i = 1.02\,\text{mW}$, $t_S = 23\,\text{ns}$, $t_R = 63\,\text{ns}$, $W_S = 1\,\text{ns}$, $W_R = 1\,\text{ns}$, $M = N = 4$, $\eta L = 2.3$, $P_{S\text{sat}} = 10\,\text{mW}$, $P_{R\text{sat}} = 11.8\,\text{mW}$, and integration step size $\Delta t = 2\,\text{ps}$. In addition, $P_0 = 0.02\,\text{mW}$; the holding-beam input is constant for flip-flop simulations, and therefore the adiabatic-approximation condition that $h(t)$ vary slowly is always satisfied. Simulations agree qualitatively with experimental data,[10] and therefore they reinforce the understanding of the physical processes described earlier this section. The model can also be applied to understand the response of the flip-flop under a variety of operation conditions, as done in Section 4.

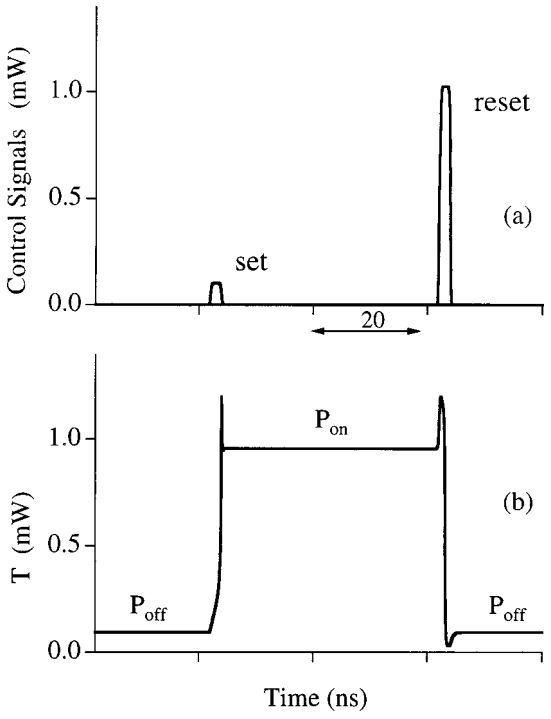

Fig. 5. Flip-flop operation using XPM: (a) set and reset signals control (b) the bistable transmission T by varying the hysteresis curve according to Figs. 3 and 4.

4. SET-SIGNAL EFFECTS

We recently demonstrated an all-optical flip-flop that uses XPM-based control techniques, and we discussed the wavelength range, power requirement, polarization sensitivity, and switching speed of the flip-flop.[10] Because set signals have a wide wavelength range (>35 nm) and operate at powers as low as 22 μW, we envision that the flip-flop can be set by data signals taken directly from a wavelength-division multiplexed optical network. We are therefore interested in the response of the flip-flop to different set-pulse conditions. In this section, we investigate how the flip-flop depends on the set-pulse power and how it responds to back-to-back set signals, and we compare the relative strength of the set and reset processes.

A. Experimental System

Set-pulse effects were explored by using the system shown in Fig. 6. Within the flip-flop (central box), we used a commercial DFB laser driven near 97% lasing threshold as the resonant-type SOA. The photonic bandgap occurred ~20 nm shorter than the gain-peak wavelength of 1567 nm, and the dominant Bragg resonance (determined by the grating phase at device facets) of the device occurred near the center of the photonic bandgap.

The holding beam was fixed at a constant input power into the SOA, its polarization was aligned with the transverse-electric mode of the SOA gain region, and its wavelength was tuned to 1547.73 nm. The Bragg resonance, which shifts to either side of the holding-beam wavelength during flip-flop operation, was initially tuned 0.124 nm to the short-wavelength side of the holding

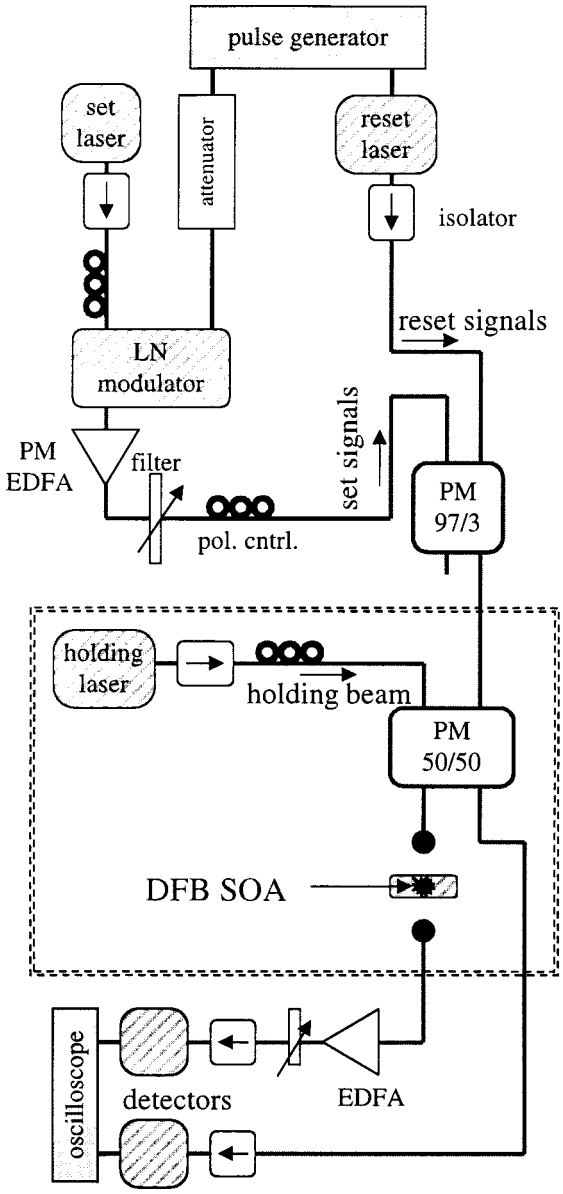

Fig. 6. Experimental setup. Dashed box indicates the flip-flop circuit. LN, lithium niobate.

beam. The flip-flop functioned properly over a holding-beam wavelength range of 0.004 nm (for a constant input power); we expect that this range can be improved by using a chirped-grating DFB SOA.[3]

Set and reset pulse trains were created by using the same pulse generator, and they were separated in time by traversing different path lengths. Directly modulated 1.31-μm reset pulses were passed through the dominant port of a 97/3 pulse-modulated (PM) fiber coupler. Then, 1537-nm set signals were externally modulated with a lithium niobate (LN) modulator and were passed through the 3% port and thus required an erbium-doped fiber amplifier (EDFA) to boost their power. The output power from the flip-flop was amplified by an EDFA and filtered to remove the set pulses and wideband amplified spontaneous emission. All signals were measured with detectors having bandwidths exceeding 20 GHz and a 500-MHz real-time oscilloscope.

B. Set-Pulse Power

Because small powers (<0.1 mW) are sufficient to set the flip-flop, data signals from an optical network can easily exceed the minimum required set power. Using the system described above, we explored how the shape of the holding-beam output power is effected by a varied set-pulse power.

Although flip-flop operation still occurs between two flat output states P_{on} and P_{off}, an intermediate state P_x can appear during the duration of the set signal. With the use of rectangular set pulses (width $\approx$ 4 ns), this intermediate state takes the form of a flat ledge, as seen in Fig. 7(a) for a set power of 0.28 mW and a holding-beam input power of 0.04 mW. We analyze the set-pulse ledge by first noting that the flat level of the ledge indicates that the system has achieved a steady state during the application of the set pulse. Thus, we can study this behavior by observing the bistable hysteresis curve using a CW set signal, as was used in Figs. 3 and 4 during the discussion on set and reset operation.

Using simulations, we find that a relatively large set-signal power (P_{S0} = 0.28 mW) pushes the upward-switching threshold well beyond the holding-beam input power P_H, as seen in Fig. 7(b), where we have overlapped the bistable hystereses with and without the set signal. (All other parameters values are the same as in Fig. 3.) The higher branch of the hysteresis drops accordingly, and therefore the output power switches from P_{off} to P_x; the intermediate state P_x is significantly lower than the final state P_{on}, which is obtained after the set pulse passes through the device.

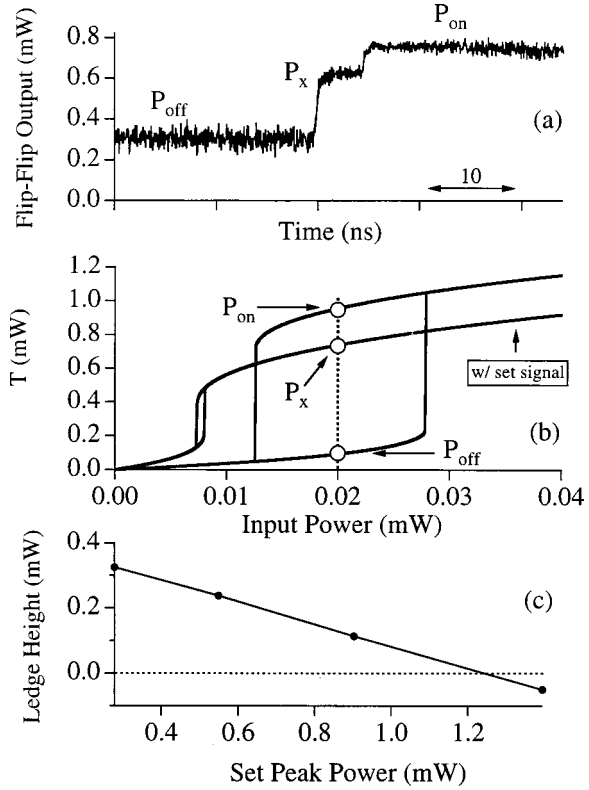

Fig. 7. Set-pulse ledge: (a) ledge feature P_x can occur during the application of the set pulse. (b) Severe hysteresis shift is the origin of the ledge. (c) Ledge height $P_x - P_{off}$ decreases with set power.

The large difference between the upper branches of each hysteresis arises from both dispersive and gain-related effects; increased XPM pushes the Bragg resonance away from the holding-beam wavelength, and larger gain saturation diminishes the strength of the Bragg resonance. These effects grow as the set-pulse power is increased. Therefore, the height of the ledge above the lower state $P_x - P_{\text{off}}$ diminishes as the set power increases, as shown in Fig. 7(c).

For a small range of set-pulse powers, the ledge height $P_x \approx P_{\text{off}}$, and the ledge is not visible. The ledge also goes unnoticed for low set powers, where $P_x \approx P_{\text{on}}$ because the flip-flop is set without too much variation in the hysteresis-branch height. Otherwise, set-pulse ledges will occur. Such ledges significantly warp the flip-flop output if their width is of the same order as the interval between set and reset signals. Relatively short set signals, however, do not significantly distort the holding-beam output shape.

C. Back-to-Back Set Signals

Because set signals are envisioned to come directly from the optical system, there may be situations in which multiple set signals enter the flip-flop before reset occurs. (All such signals are referred to here as set signals, although only the first one sees the flip-flop in its off state.) The stability and response of the flip-flop output power to back-to-back signals is therefore important to consider.

A pulse sequence of two set signals followed by a reset signal is used in experiments, as shown in Fig. 8(a), where the holding-beam power $P_H = 0.068\,\text{mW}$; the response of the flip-flop is shown in Fig. 8(b). The first and last pulses of this sequence perform set and reset, as expected. A ledge was produced for a set power of 0.59 mW, as described above.

While the holding beam is in the high-output state P_{on}, the second set signal enters the SOA. The flip-flop output power is reduced for the duration of the set signal, but it returns to P_{on} after the signal dissipates. The notch in the output power can also be understood from the hystereses in Fig. 7(b) used to describe the set-pulse ledges. Unlike for the case of the ledges, however, the holding-beam output power begins in the high state P_{on}. The second set signal pushes the hysteresis curve to smaller switching powers, and the output power drops accordingly to P_x. However, because the switching thresholds do not cross the holding-beam input power, the final output state does not change; after the set pulse dissipates, the hysteresis curve returns to original shape with the holding-beam output power at P_{on}.

Using the theoretical model, we simulated the flip-flop response to back-to-back set pulses. Both set-pulse ledges and notches are obtained, as shown in Fig. 9, where the parameter values are the same as in Fig. 5, except $S_i = 0.6\,\text{mW}$, $R_i = 2.2\,\text{mW}$, $W_S = 0.8\,\text{ns}$, $W_R = 0.6\,\text{ns}$, and $t_R = 66\,\text{ns}$. The second set signal is defined by $S_i = 0.6\,\text{mW}$, $W_S = 0.8\,\text{ns}$, and $t_s = 42\,\text{ns}$. The set and reset switching exhibit spikes, as seen for numerical data shown in Fig. 5. Spiking behavior of this sort is common in simulations of dispersive bistability,[2,8,14] and it occurs as the holding beam passes through the peak of the Bragg resonance. Enhancement of spikes in simulations occurs as an artifact from the adiabatic elimination of the bistable signal from the system dynamics.[8] Furthermore, suppression of spikes in experimental measurements has been attributed to the slow response of the de-

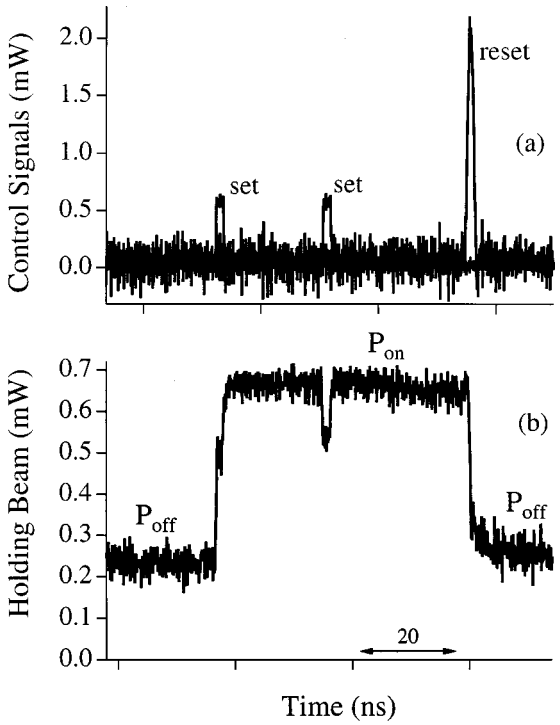

Fig. 8. Back-to-back set signals: (a) control signals; an additional set pulse enters the DFB SOA between set and reset signals. (b) In response, the holding-beam transmission remains stable and only experiences a transient dip.

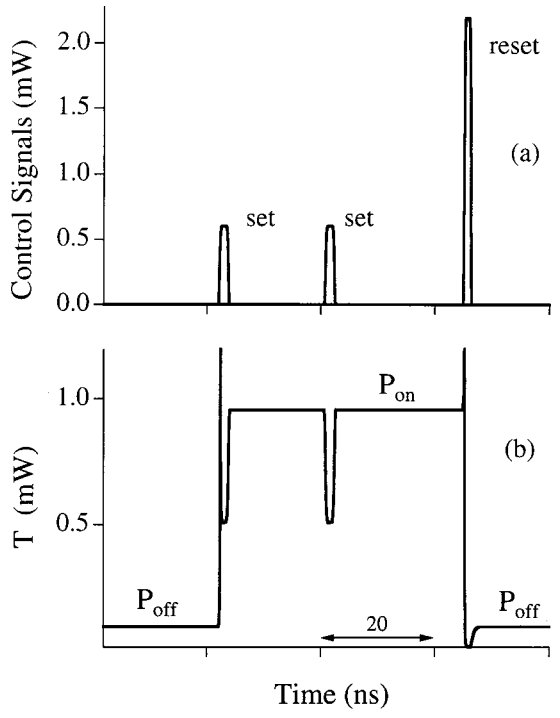

Fig. 9. Simulated response of the flip-flop to back-to-back set signals: (a) control signals; (b) holding-beam transmitted power, showing a ledge and a notch.

tection scheme[14]; our 500-MHz oscilloscope may have diminished the measured spikes.

Figure 9 also reveals a notch during reset operation; this momentary decrease in power occurs as the reset pulse shifts the Bragg resonance away from the holding-beam wavelength. The reset notch, however, is not observed in the experimental data of Fig. 8; we believe that the notch is masked by the excess spontaneous emission contributed by the Bragg resonance, which is strengthened during the application of the reset pulse. This noise feature is beyond the scope of our simple model.

In our experiments, which used peak signal powers of ~0.6 mW and widths of ~4 ns, the second set pulse never caused the holding-beam power to become unstable and return to the lower level P_{off}. Moreover, if the output power from the flip-flop is coupled into an optical network, fiber dispersion will fill in the notches caused by set pulses that are short compared with the on-state duration. In this case, back-to-back set signals have no lasting effect.

D. Set-Signal Strength

In experiments and simulations, we found that the required set-signal power is much smaller than that of the reset signal. The theoretical model presented here provides insight into the relative strength of these processes. The phase change $\Delta\phi$, experienced by the holding beam as the gain changes by an amount Δg, is given by the change in wave number, $\Delta\phi = -\Delta g L\alpha/2$. Using the steady-state solution to gain rate equation (22), and isolating the effects of the optical signals, we find that the phase change is given by

$$\Delta\phi = \frac{\alpha}{D_\phi}\left[\frac{g_0 L}{2}\frac{\langle P_A\rangle + \langle P_B\rangle}{P_{\mathrm{sat}}} + \frac{g_0 L}{2}\frac{\langle P_S\rangle}{P_{S\mathrm{sat}}} - \frac{\eta L}{2}\frac{\langle P_R\rangle}{P_{R_{\mathrm{sat}}}}\right], \tag{33}$$

$$D_\phi = 1 + \frac{\langle P_A\rangle + \langle P_B\rangle}{P_{\mathrm{sat}}} + \frac{\langle P_S\rangle}{P_{S\mathrm{sat}}}. \tag{34}$$

The three terms in the bracketed expression of Eq. (33) represent (from left to right) holding-beam SPM, set-signal XPM $\Delta\phi_{S\mathrm{XPM}}$, and reset-signal XPM $\Delta\phi_{R\mathrm{XPM}}$. For the parameter values used throughout this paper ($\alpha = 5$, $g_0 L \approx 1.2$, and $\eta L = 2.3$), the prefactors are $\alpha g_0 L/2 \approx \pi$ and $\alpha\eta L/2 \approx 2\pi$. Thus, the strength of each signal power (within the SOA) relative to its saturation power determines the number of π phase shifts experienced by the holding beam.

For the case of small optical powers (relative to the saturation powers), the quantity $D_\phi \approx 1$. The expression for set-signal XPM can be estimated by using average-power equation (29) with the small-signal limit $g = g_0$ and $P_{S\mathrm{sat}} = 10\,\mathrm{mW}$:

$$\Delta\phi_{S\mathrm{XPM}} \approx 0.18\pi P_{S0}, \tag{35}$$

$$\Delta\phi_{R\mathrm{XPM}} \approx -0.06\pi P_{R0}. \tag{36}$$

The phase change for the reset signal $\Delta\phi_{R\mathrm{XPM}}$ was obtained by using Eq. (29) for the average power and $P_{R\mathrm{sat}} = 11.8\,\mathrm{mW}$.

To obtain the same phase shift, relations (35) and (36) reveal that the reset signal must provide more power than the set signal. In addition to having a smaller saturation power, the set signal is amplified by the medium, as opposed to the absorption of the reset signal. Moreover, the effect of the holding-beam power on XPM (i.e., $D_\phi > 1$) makes the difference in required powers even greater; whereas the set signal sees a relatively small internal holding-beam power, the reset signal sees a resonant-amplified holding beam, further reducing $\Delta\phi_{R\mathrm{XPM}}$.

5. CONCLUSION

We describe all-optical techniques for setting and resetting a SOA-based optical flip-flop. Instead of varying the holding-beam input power (SPM), we vary the bistable hysteresis curve itself by using auxiliary control signals (XPM) that shift the photonic bandgap and Bragg resonances.

These set–reset techniques exploit yet another remarkable aspect of SOA's—optical signals can be used either to increase *or* decrease the refractive index. These XPM processes occur over a wide wavelength range and at reasonable optical powers, ensured by the strong SOA carrier nonlinearity. The flip-flop technology also has the advantage of maturity and potential for photonic-circuit integration—experiments were performed by using a commercially available telecommunications diode laser (driven below lasing threshold).

Accompanying the strong SOA carrier nonlinearity, however, is a carrier lifetime $\tau \sim 0.2$–1 ns,[16] which limits the repetition rate of the flip-flop. Electrical and optical bias techniques have been used to shorten the effective lifetime of SOA's down to 10 ps;[17] we expect that these techniques permit flip-flop operation at data rates of 10 Gb/s and faster. In addition, pulses shorter than the carrier lifetime can set and reset the flip-flop; this feature can be exploited for applications such as format conversion from high-speed (>10 Gb/s) return-to-zero to low-speed nonreturn-to-zero data.[18]

The theoretical model used to describe flip-flop operation incorporates the bistable system and control signals. To arrive at a simple equation, we invoke approximations that are common to the study of optical bistability and to nonlinear SOA dynamics; our simulations are in qualitative agreement with experiments that use back-to-back set signals and a varied set-pulse power. We expect the present model to be useful for further investigation into the response of the flip-flop, as well as for applications to fiber-optic communication systems.

ACKNOWLEDGMENTS

D. Maywar greatly appreciates discussions with D. Aronstein, M. Tsurusawa, Y. Katagiri, M. Funabashi, T. Yamaguchi, K. Shimizu, and T. Yasui. We thank D. Inoue and M. Kato for their technical assistance. This research was supported by the U.S. National Science Foundation (Grant INT-9809932), the International Communication Foundation, and the Telecommunications Advancement Organization of Japan.

The authors can be reached at the addresses on the title page. D. Maywar may be reached by e-mail at maywar@optics.rochester.edu.

REFERENCES

1. H. G. Winful, J. H. Marburger, and E. Garmire, "Theory of bistability in nonlinear distributed feedback structures," Appl. Phys. Lett. **35**, 379–381 (1979).
2. M. J. Adams and R. J. Wyatt, "Optical bistability in distributed feedback semiconductor laser amplifiers," IEE Proc. **134**, 35–40 (1987).
3. D. N. Maywar and G. P. Agrawal, "Effect of chirped gratings on reflective optical bistability in DFB semiconductor laser amplifiers," IEEE J. Quantum Electron. **34**, 2364–2370 (1998).
4. G. P. Agrawal and N. K. Dutta, *Semiconductor Lasers*, 2nd. ed. (Van Nostrand Reinhold, New York, 1993).
5. G. P. Agrawal and N. A. Olsson, "Self-phase modulation and spectral broadening of optical pulses in semiconductor laser amplifiers," IEEE J. Quantum Electron. **25**, 2297–2306 (1989).
6. H. Kawaguchi, "Progress in optical functional devices using two-section laser diodes/amplifiers," IEE Proc. **140**, 3–15 (1993).
7. R. J. Manning, A. D. Ellis, A. J. Poustie, and K. J. Blow, "Semiconductor laser amplifiers for ultrafast all-optical signal processing," J. Opt. Soc. Am. B **14**, 3204–3216 (1997).
8. N. Ogasawara and R. Ito, "Static and dynamic properties of nonlinear semiconductor lasers amplifiers," Jpn. J. Appl. Phys. **25**, 739–742 (1986).
9. K. Inoue, "All-optical flip-flop operation in an optical bistable device using two lights of different frequencies," Opt. Lett. **12**, 918–920 (1987).
10. D. N. Maywar, G. P. Agrawal, and Y. Nakano, "Robust optical control of an optical-amplifier-based flip-flop," Opt. Express **6**, 75–80 (2000).
11. H. Kogelnik and C. V. Shank, "Coupled-wave theory of distributed feedback lasers," J. Appl. Phys. **43**, 2327–2335 (1972).
12. K. Otsuka and H. Iwamura, "Analysis of a multistable semiconductor light amplifier," IEEE J. Quantum Electron. **19**, 1184–1186 (1983).
13. P. Meystre, "On the use of the mean-field theory in optical bistability," Opt. Commun. **26**, 277–280 (1978).
14. W. F. Sharfin and M. Dagenais, "Dynamics of optically switched bistable diode laser amplifiers," IEEE J. Quantum Electron. **23**, 303–308 (1987).
15. T. Durhuus, C. Joergensen, B. Mikkelsen, R. J. S. Pedersen, and K. E. Stubkjaer, "All optical wavelength conversion by SOA's in a Mach-Zehnder configuration," IEEE Photonics Technol. Lett. **6**, 53–55 (1994).
16. M. J. Adams, D. A. O. Davies, M. C. Tatham, and M. A. Fisher, "Nonlinearities in semiconductor laser amplifiers," Opt. Quantum Electron. **27**, 1–13 (1995).
17. R. J. Manning, and D. A. O. Davies, and J. K. Lucek, "Recovery rates in semiconductor laser amplifiers: optical and electrical bias dependencies," Electron. Lett. **30**, 1233–1234 (1994).
18. D. N. Maywar, Govind P. Agrawal, and Y. Nakano, "Robust all-optical control of a semiconductor optical amplifier flip-flop," presented at Optical Amplifiers and Their Applications, Quebec, Canada, July 9–12, 2000.